ACS Catalysis

pubs.acs.org/acscatalysis

Research Article

Electrocatalytic Water Oxidation with α-[Fe(mcp)(OTf)$_2$] and Analogues

Silvia D'Agostini, Konstantin G. Kottrup, Carla Casadevall, Ilaria Gamba, Valeria Dantignana, Alberto Bucci, Miquel Costas,* Julio Lloret-Fillol,* and Dennis G.H. Hetterscheid*

Cite This: *ACS Catal.* 2021, 11, 2583–2595

Read Online

ACCESS | Metrics & More | Article Recommendations | Supporting Information

ABSTRACT: The complex α-[Fe(mcp)(OTf)$_2$] (mcp = *N*,*N*′-dimethyl-*N*,*N*′-bis-(pyridin-2-ylmethyl)-cyclohexane-1,2-diamine and OTf = trifluoromethanesulfonate anion) was reported in 2011 by some of us as an active water oxidation (WO) catalyst in the presence of sacrificial oxidants. However, because chemical oxidants are likely to take part in the reaction mechanism, mechanistic electrochemical studies are critical in establishing to what extent previous studies with sacrificial reagents have actually been meaningful. In this study, the complex α-[Fe(mcp)(OTf)$_2$] and its analogues were investigated electrochemically under both acidic and neutral conditions. All the systems under investigation proved to be electrochemically active toward the WO reaction, with no major differences in activity despite the structural changes. Our findings show that WO-catalyzed by mcp−iron complexes proceeds via homogeneous species, whereas the analogous manganese complex forms a heterogeneous deposit on the electrode surface. Mechanistic studies show that the reaction proceeds with a different rate-determining step (rds) than what was previously proposed in the presence of chemical oxidants. Moreover, the different kinetic isotope effect (KIE) values obtained electrochemically at pH 7 (KIE ∼ 10) and at pH 1 (KIE = 1) show that the reaction conditions have a remarkable effect on the rds and on the mechanism. We suggest a proton-coupled electron transfer (PCET) as the rds under neutral conditions, whereas at pH 1 the rds is most likely an electron transfer (ET).

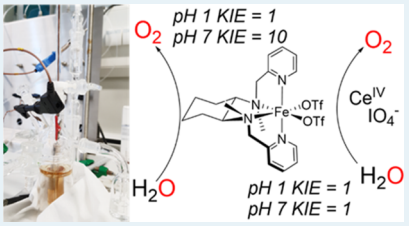

KEYWORDS: *water oxidation, iron complexes, manganese complexes, electrocatalysis, chemical oxidants, isotope effects*

INTRODUCTION

The goal of reducing the world energy problems by moving away from fossil fuels has raised ever-growing interest in the search for renewable energy sources. Solar energy is a well-known and promising source, and can be harvested in sufficient amounts to power the planet.[1] Because of intermittency reasons, it is important to store excess solar energy in the form of a chemical fuel. This can be achieved by splitting water into O_2 and H_2.[1] In order to make water splitting more efficient, a better understanding of the catalytic water oxidation (WO) process is required. Thus far, many research groups have directed their attention to the development of catalysts based on transition metals that are able to perform efficient WO. The complexes that are proved to be the most active are based on ruthenium[2−11] and iridium.[12−18] Ruthenium-based catalysts exhibited turnover numbers (TONs) exceeding 10^6,[19] turnover frequencies (TOFs) in the range of 5×10^4 s^{-1},[5,19] and an overpotential of 180 mV.[20] Iridium-based catalysts showed TONs exceeding 10^6 with an overpotential of 250 mV.[21] However, an important requirement toward sustainability is the use of earth-abundant elements.[22,23] In this regard, iron is biocompatible, abundant, has a rich redox chemistry, and plays a prominent role in oxidation chemistry. Several iron complexes have been developed that can act as molecular water oxidation catalysts.[24−36] Collins and co-workers developed the Fe−TAML (TAML = tetra-amido macrocyclic ligand) systems, which exhibited a TOF value of 1.3 s^{-1}.[24] Masaoka *et al.* reported a pentanuclear iron catalyst showing a remarkable turnover frequency of 1900 s^{-1}.[32] Some of us developed iron-based homogeneous water oxidation catalysts, which yielded TONs of about 3400 and TOFs of 0.4 s^{-1}.[25,37,38] However, most of the catalysts mentioned have been studied in the presence of chemical oxidants, such as cerium ammonium nitrate (CAN) and sodium periodate ($NaIO_4$).[25,37,39−43] When using chemical oxidants, the choice of the reaction conditions is limited to the stability of the oxidant, which lies in a limited pH region, and no redox-potential control can be achieved. Furthermore, it has been shown that these oxidants can take active part in the reaction mechanism.[25,37,41] In this regard, electrochemical methods are crucial to elucidate whether the observed catalytic properties are actually independent of sacrificial oxidants. Recently, some of us used electrochemical methods coupled with mass spectrometry to

Received: December 11, 2020
Revised: January 26, 2021
Published: February 11, 2021

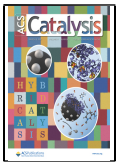

study metal-catalyzed WO reactions. Fe(cyclam) (cyclam = 1,4,8,11-tetraazacyclotetradecane) complexes with two cis vacant sites or having a fifth donor axial ligand and the dinuclear iron complex $[\{(MeOH)Fe(Hbbpya)\}_2(\mu-O)](OTf)_4$ (Hbbpya = *N*,*N*-bis(2,2′-bipyrid-6-yl)amine) were found to be electrocatalytically active toward WO.[31,33] In the latter case, further studies benchmarked an overpotential of 300−400 mV and a TOF of 0.12 s^{-1}. On the other hand, electrochemical studies with $[\{(MeOH)Fe(Hbbpya)\}_2(\mu-O)](OTf)_4$ have also shown that the choice of the electrode material is important as the complex exhibited enhanced water oxidation activity in combination with graphitic working electrodes.[33]

In this study, we have investigated α-$[Fe(mcp)(OTf)_2]$ (mcp = *N*,*N*′-dimethyl-*N*,*N*′-bis(pyridin-2-ylmethyl)-cyclohexane-1,2-diamine; OTf = trifluoromethanesulfonate anion), the Fe^{III} analogue α-$[Fe(mcp)(Cl)_2]Cl$, the deuterated analogue α-$[Fe(D4\text{-}mcp)(OTf)_2]$, β-$[Fe(mcp)(OTf)_2]$, and the manganese coordination complex α-$[Mn(mcp)(OTf)_2]$ as WO electrocatalysts (Chart 1). Our findings show that water

Chart 1. Iron and manganese complexes evaluated in this study.

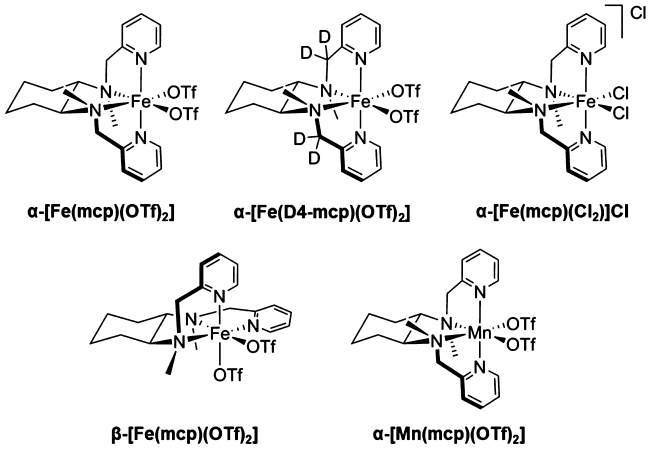

oxidation catalyzed by mcp iron complexes proceeds via homogeneous species, also under electrocatalytic conditions, and that a proton transfer is involved in the rate-determining step (rds). In contrast, the analogue Mn complex α-$[Mn(mcp)(OTf)_2]$ forms a heterogeneous deposit on the electrode surface instead.

RESULTS

Voltammetry under Neutral and Acidic Conditions. First, we examined the behavior of complex α-$[Fe(mcp)(OTf)_2]$ by cyclic voltammetry (CV) in aqueous $NaClO_4$ (0.1 M) and Na_2SO_4 (0.1 M) electrolyte solutions. In both electrolyte solutions, identical results were obtained showing a reversible redox couple at 0.8 V versus RHE. The cyclic voltammogram (CV) recorded with a glassy carbon electrode (GC) from 0 to 2 V (all potentials are given vs RHE unless otherwise specified) shows a reversible redox wave at 0.8 V assigned to the Fe^{II}/Fe^{III} redox couple (Figure 1), and an irreversible oxidation wave starting at about 1.7 V, which could be attributed to WO electrocatalytic activity. Very similar results were obtained using basal plane pyrolytic graphite (PG) and boron-doped diamond (BDD) as working electrodes (Figure S1), while the electrochemistry of α-$[Fe(mcp)(OTf)_2]$

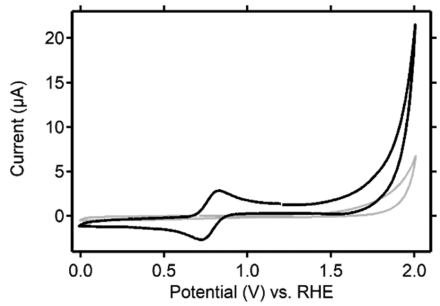

Figure 1. CV in the presence (black) and the absence (gray) of α-$[Fe(mcp)(OTf)_2]$ (1 mM) in 0.1 M Na_2SO_4, scanning at 20 mV/s, using a GC working electrode.

using a gold working electrode is more complex because of the oxidation of the gold surface (Figure S1). The advantage of BDD is that very small background currents are recorded, yet not useable for some applications because of very slow electron transfer processes. In contract, the PG, fluorine-doped tin oxide (FTO), and gold electrodes used are more appropriate for bulk electrolysis applications, which will be discussed later.

Heterogeneous iron-based materials such as Fe_2O_3 are known to be active water oxidation catalysts[44−47] and may potentially form through the decomposition of homogeneous complexes under the harsh oxidative conditions applied. The potential formation of catalytically active heterogeneous materials is a constant concern in the field of homogeneous WO catalysis.[48] In this regard, electrochemical quartz crystal microbalance (EQCM) methods have been found useful to rule out the formation of catalytically active heterogeneous species that may become deposited at the surface of working electrodes.[49,50] The working electrode in EQCM experiments consists of a thin layer of gold, deposited on a quartz crystal oscillator. Mass changes at the working electrode can be detected by measuring the changes in the resonance frequency of the quartz crystal.[51] To avoid damaging the thin gold layer of the EQCM electrode and because of the mass change associated with gold oxide formation and reduction, the potential was kept above 1.3 V during EQCM experiments to avoid gold oxide reduction. To understand the nature of the catalytically active species, we have performed an EQCM experiment between 1.3 and 2.0 V at 1 mV/s, recorded in the presence of α-$[Fe(mcp)(OTf)_2]$ (pH = 7; Figure 2). The first scan of the experiment (Figure 2a) shows an increase in the oscillation frequency, which translates into an apparent decrease in mass of the electrode. This observation has been previously attributed to bubble-formation at the working electrode, which causes changes in hydrophobicity of the solute.[52] After the initial increase in oscillation frequency during the first scan, no further changes in frequency take place in subsequent scans, which indicates that catalytically active species stay homogeneous and suggests that they are molecular in nature. In contrast to the results obtained with α-$[Fe(mcp)(OTf)_2]$, an EQCM experiment conducted in the presence of $Fe(OTf)_2$ shows a clear decrease in oscillation frequency, which is consistent in both the first and second scans and indicates the formation of a deposit on the surface of the gold electrode (Figure 2b).[33]

To assess the WO capabilities of α-$[Fe(mcp)(OTf)_2]$, online electrochemical mass spectrometry (OLEMS) experiments were carried out in combination with CV. In OLEMS measurements, the gaseous products are sampled close to the

https://dx.doi.org/10.1021/acscatal.0c05439
ACS Catal. 2021, 11, 2583−2595

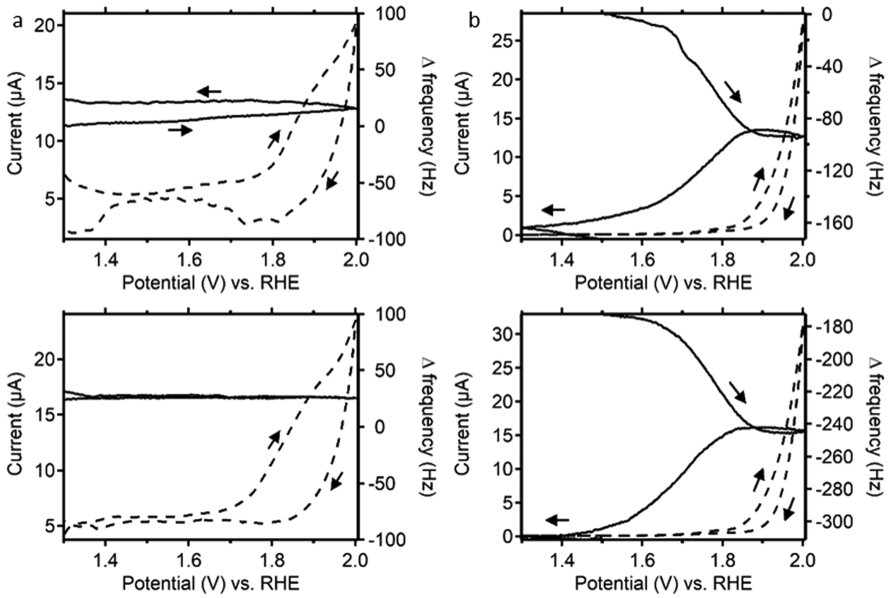

Figure 2. CV in combination with quartz crystal microbalance (EQCM) experiment at a gold working electrode, cycling the potential between 1.3 and 2.0 V vs RHE at 1 mV/s. (a) CVs and frequency changes of α-[Fe(mcp)$(OTf)_2$] (1.1 mM) in aqueous $NaClO_4$ (0.1 M). Shown are the first scan (top) and third scan (bottom) of the EQCM experiment. (b) CVs and frequency changes of $Fe(OTf)_2$ (1.0 mM) in aqueous Na_2SO_4 (0.1 M). Shown are the first scan (top) and second scan (bottom) of the EQCM experiment. Solid lines represent the frequency trace and the current is given in dashed lines. Arrows indicate the direction of the scan. Figure 2b top was reprinted with permission from ref 33.

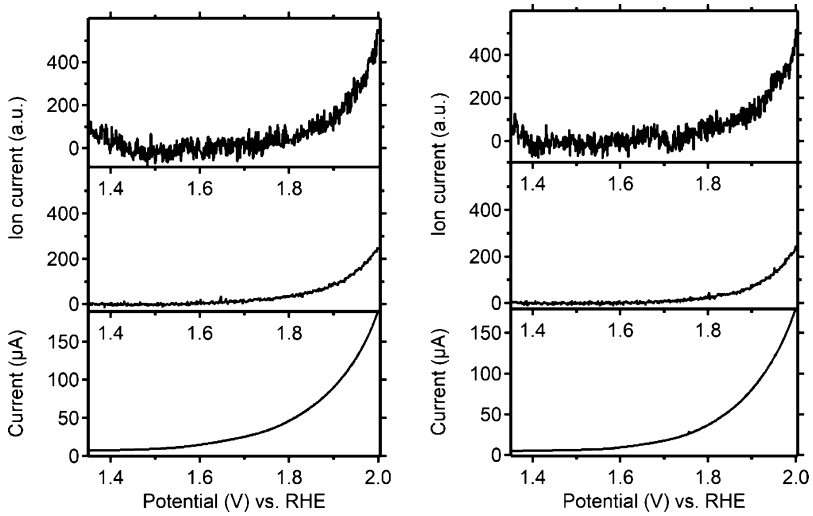

Figure 3. CV in combination with OLEMS of α-[Fe(mcp)$(OTf)_2$] (1.1 mM) in 0.1 M $NaClO_4$ using a PG working electrode at a scan rate of 1 mV/s. Depicted are the m/z traces of O_2 (top), CO_2 (middle), and the corresponding current (bottom). The forward sweep of both the first scan (left) and the second scan (right) is shown.

electrode surface in solution and selected m/z values are recorded as a function of the applied potential.[53] During all OLEMS experiments, m/z = 32 and 44 were recorded to monitor the oxygen evolution reaction and possible oxidative decomposition of the ligand (CO_2 formation) under the strongly oxidizing conditions applied.[48,54−56] In all OLEMS experiments, the potential was cycled between 1.3 and 2.0 V at 1 mV/s for a total of three cycles. Herein, rough PG electrodes were used, which allow for a sufficiently large production of O_2 per cm^2 geometric surface area for detection by OLEMS.

In OLEMS experiments with a PG working electrode, α-[Fe(mcp)$(OTf)_2$] demonstrates WO activity (Figure 3). In the current trace, an oxidative current can be seen starting at 1.7 V with a sharp increase at about 1.8 V. The mass traces for O_2 and CO_2 measured during the OLEMS experiment show onsets at about 1.8 V.

The formation of CO_2 has been routinely detected in OLEMS experiments with a PG working electrode for all metal complexes studied in our group and even in the absence of any metal complex in solution (see Figure S2).[31,33] To clarify the origin of the observed CO_2 formation during the experiment with α-[Fe(mcp)$(OTf)_2$], an additional OLEMS experiment was performed with a gold working electrode. Although the first CV scan shows additional features because of the formation of gold oxide, the experiment excludes the mcp ligand as the source of CO_2. In a second scan and subsequent scans of the OLEMS experiment on gold, in the presence of α-[Fe(mcp)$(OTf)_2$], a sharp increase in the recorded current is

https://dx.doi.org/10.1021/acscatal.0c05439
ACS Catal. 2021, 11, 2583−2595

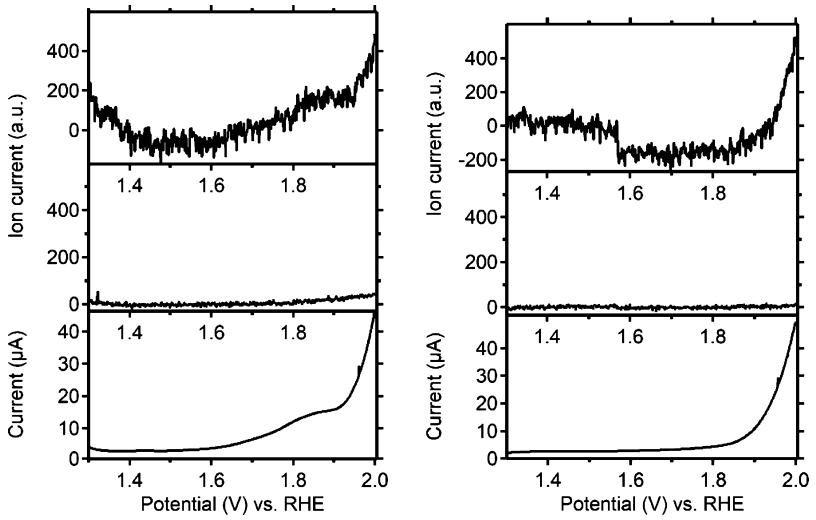

Figure 4. CV in combination with OLEMS of α-[Fe(mcp)(OTf)$_2$] (1.1 mM) in 0.1 M $NaClO_4$ using a gold working electrode at a scan rate of 1 mV/s. Depicted are the m/z traces of O_2 (top) CO_2 (middle) and the corresponding current (bottom) as a function of applied potential. The forward sweep of the first scan showing a gold oxidation wave at 1.8 V vs RHE (left) and the second scan (right) is shown.

visible, starting between 1.8 and 1.9 V. The mass trace for m/z = 32 shows an onset of dioxygen evolution, which correlates with the oxidative current while the mass trace for m/z = 44 shows no signs of CO_2 formation (Figure 4). The onset of dioxygen formation appears to be slightly delayed in the OLEMS experiments with a gold working electrode compared to the experiments with a PG working electrode. However, the contribution of CO_2 formation to the current in the experiment with a PG electrode makes it more difficult to precisely determine the onset of dioxygen evolution. The lack of CO_2 formation in the experiment with a gold working electrode on the other hand indicates that the CO_2 formation observed for the case of a PG working electrode is mainly because of the oxidation of the electrode material itself.

In addition to qualitative measurements to determine the oxygen production as a function of applied potential, also quantitative bulk experiments were performed to determine the Faradaic efficiency of the water oxidation reaction. A Faradaic Yield (FY) of 87% was obtained when an FTO electrode was used (Figure 5), while the FYs dropped significantly when carbon-based electrodes were used instead.

Because previous studies showed that α-[Fe(mcp)(OTf)$_2$] shows good catalytic rates under acidic conditions in the presence of CAN, we decided to also investigate the complex by means of electrochemistry under acidic conditions. However, the Fe(II) complex is not stable for extended periods at low pH because of demetallation. Demetallation at low pH is not an issue for the catalytic water oxidation experiments performed with CAN because upon addition of CAN, the Fe(II) complex is quickly oxidized to higher oxidation states, which are significantly more stable against demetallation (vide infra). However, in electrochemical experiments, the bulk of the complex present in solution remains in the Fe(II) resting-state throughout the experiment. As a result, demetallation occurs, causing noticeable degradation of the complex on the time scale of the electrochemical experiments. Previous studies showed that α-[Fe(mcp)(OTf)$_2$] is hydrolyzed at low pH such as in solutions of 0.1 M triflic acid.[42,57] The ligand demetallation in the iron(II) precursor is too fast to exclude free iron in solution, which potentially can affect the CV (Figures S3 and S4a). However,

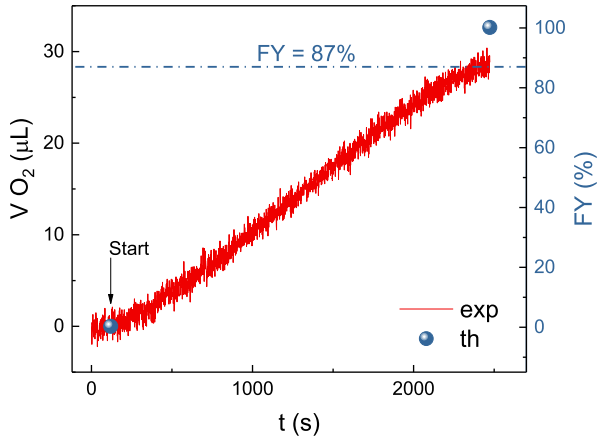

Figure 5. Determination of O_2 produced (red line) and FY (blue dots) for α-[Fe(mcp)(OTf)$_2$] during chronoamperometry experiment (E = 1.8 V vs RHE, 30 min) monitored using an oxygen sensor probe. The blue-dashed line represents the FY measured. In this experiment, α-[Fe(mcp)(OTf)$_2$] was used at a concentration of 1.1 mM, in 10 mM phosphate buffer at pH 6.8.

having the iron center in the +III oxidation state beforehand prevents the ligand dissociation. According to UV−vis experiments, the iron(III) complex α-[Fe(mcp)(Cl)$_2$]Cl is stable in the acidic electrolyte (pH 1, 0.1 M H_2SO_4, Figure 6).

Concordantly, we have investigated the electrochemistry of α-[Fe(mcp)(Cl)$_2$]Cl under both neutral and acidic conditions (Figures S6 and 7). In contrast to the CV studies in the presence of α-[Fe(mcp)(OTf)$_2$], solutions of α-[Fe(mcp)(Cl)$_2$]Cl produce multiple redox couples between 0.5 and 1.2 V versus RHE. This suggests the presence of multiple species in solution, probably as a result of dimerization or partly (de)coordination of chloride. The oxidation of chloride can be ruled out, given that this process takes place at a significantly higher redox potential.

OLEMS experiments of α-[Fe(mcp)(Cl)$_2$]Cl were carried out in both 0.1 M Na_2SO_4 and 0.1 M H_2SO_4 electrolyte solutions. The presence of chloride anions in α-[Fe(mcp)(Cl)$_2$]Cl is not compatible with a gold electrode at potentials exceeding 1.2 V versus RHE because of the facile formation of

https://dx.doi.org/10.1021/acscatal.0c05439
ACS Catal. 2021, 11, 2583−2595

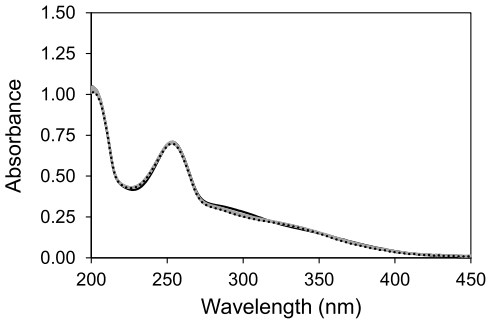

Figure 6. Evolution of the UV−vis absorption of α-[Fe(mcp)$(Cl)_2$]Cl (0.05 mM) in a 0.1 M H_2SO_4 solution over 2 h, recorded in 15 min intervals. Depicted are the UV−vis spectra recorded at t = 0 min (solid line) and at t = 120 min (dotted line) and the intermediate UV−vis spectra recorded every 15 min (gray lines).

$[AuCl_4]^{2-}$ under oxidative conditions.[31] Consequently, OLEMS experiments in the presence of α-[Fe(mcp)$(Cl)_2$]Cl were exclusively performed with a PG working electrode. The results of the OLEMS experiments of α-[Fe(mcp)$(Cl)_2$]Cl in 0.1 M Na_2SO_4 solution are qualitatively similar to those obtained from OLEMS experiments of α-[Fe(mcp)$(OTf)_2$] in 0.1 M $NaClO_4$ solution (Figure S8). In both cases, the current trace shows an oxidation wave with a sharp increase in current starting near 1.8 V. The m/z traces for both experiments show an onset of dioxygen evolution around 1.8 V, which correlates with the sharp increase in current. The onset of CO_2 formation lies above 1.8 V, correlating with the onset of oxidative current in the current trace. The OLEMS experiment of α-[Fe(mcp)-$(Cl)_2$]Cl in 0.1 M H_2SO_4 (Figure 8) shows a significantly higher current compared to that observed in 0.1 M Na_2SO_4 (Figure S8a). From 1.8 V onward, oxidative current can be seen in the current trace (Figure 8, bottom) which correlates with the onset of CO_2 formation (Figure 8, middle). The onset of dioxygen evolution lies near 1.8 V (Figure 8, top), correlating with the sharp increase in oxidative current visible in the current trace.

Structural Modifications. To further assess the stability of the WO catalysts under electrocatalytic conditions, we have also evaluated the activity of α-[Fe(D4-mcp)$(OTf)_2$] and β-[Fe(mcp)$(OTf)_2$] under electrocatalytic conditions. Previous work showed that, when driven by chemical oxidants CAN and $NaIO_4$, the deuterated analogue α-[Fe(D4-mcp)$(OTf)_2$] is considerably more robust and resistant toward ligand degradation under oxidative conditions compared to the nondeuterated analogue. We previously reported that the deuteration of the methylene positions of the mcp ligand

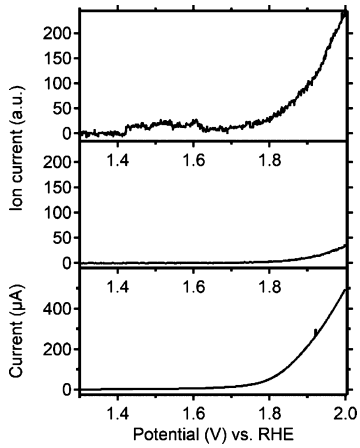

Figure 8. CV in combination with OLEMS of 1.1 mM α-[Fe(mcp)$(Cl)_2$]Cl in 0.1 M H_2SO_4 solution using a PG working electrode at a scan rate of 1 mV/s. Depicted are the m/z traces of O_2 (top), CO_2 (middle), and the corresponding current (bottom). For the sake of clarity, only the forward sweep of the second scan is shown.

produces a 10-fold increase in the stability of the $Fe^{IV}(O)$ resting state intermediate and a 5-fold increase in the water oxidation activity of the iron coordination complex.[38] β-[Fe(mcp)$(OTf)_2$] on the other hand is less stable with only 1/2 the half-life of α-[Fe(mcp)$(OTf)_2$].[37]

Considering these pronounced differences in stability of the different Fe(mcp)-analogues under catalytic conditions in the presence of chemical oxidants, we decided to investigate whether these differences translate into the realm of electrocatalysis as well. Given that the methylene backbone of the mcp ligand was shown to be unstable under strongly oxidizing conditions at reaction times of minutes to hours, we have compared the CV of the deuterated α-[Fe(D4-mcp)$(OTf)_2$] complex with that of the nondeuterated one, α-[Fe(mcp)-$(OTf)_2$]. We did not observe any significant differences in the activity and stability of both complexes under the conditions explored in this contribution (Figures S9 and S10), which confirms that under the studied catalytic conditions, the α-[Fe(mcp)$(OTf)_2$] complex is stable during the course of the experiments.

To better compare the WO catalytic activities of α-[Fe(mcp)$(OTf)_2$] and β-[Fe(mcp)$(OTf)_2$], BDD disks were used (Figure 9). The background current of the BDD electrode is relatively marginal and does not change significantly under oxidative conditions in contrast to GC and PG. The Fe^{II}/Fe^{III} redox couple of β-[Fe(mcp)$(OTf)_2$] is

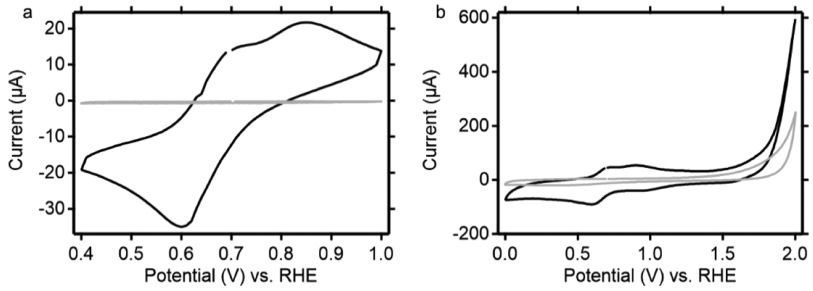

Figure 7. Voltammograms of 1.1 mM α-[Fe(mcp)$(Cl)_2$]Cl in 0.1 M H_2SO_4 solution. Shown are (a) range between 0.4 and 1.0 V vs RHE, starting at 0.7 V vs RHE, recorded with a gold working electrode and (b) range between 0.0 and 2.0 V vs RHE, starting at 0.7 V vs RHE recorded with a PG working electrode. Both voltammograms were recorded at a scan rate of 100 mV/s.

https://dx.doi.org/10.1021/acscatal.0c05439
ACS Catal. 2021, 11, 2583−2595

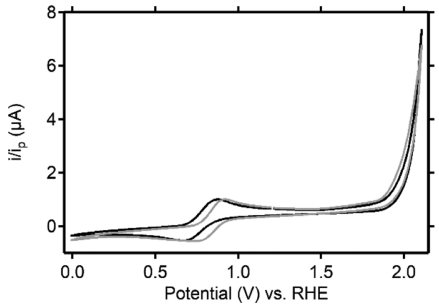

Figure 9. Voltammograms of 1 mM α-[Fe(mcp)(OTf)$_2$] (black line) and β-[Fe(mcp)(OTf)$_2$] (gray line) in 0.1 M Na_2SO_4 at a scan rate of 20 mV/s, using a BDD working electrode. For the sake of comparison, the catalytic current (i) was normalized with the peak current (i_p) of the oxidation event of the redox couple (i/i_p).

shifted 40 mV to higher potentials in comparison with α-[Fe(mcp)(OTf)$_2$]. Besides this small shift in the position of the redox couple, the two complexes show a similar current profile and onset for the water oxidation reaction.

Mechanistic Studies. Mechanistic analyses were performed to shed light on the reaction mechanism of electrocatalytic water oxidation with α-[Fe(mcp)(OTf)$_2$]. In order to determine the rate order in the catalyst, CV of α-[Fe(mcp)(OTf)$_2$] was performed at different concentrations, between 2.0 and 0.3 mM. For the calculation of the rate order, the values of the catalytic currents at different concentrations were normalized with the corresponding peak current values of the oxidation event of the redox couple. The ratio between these values, namely i_{cat}/i_p, was plotted versus the concentration. For this system, a first order rate in [Fe] was found (see Figure S11).

Next, the electrocatalytic WO activity of α-[Fe(mcp)(OTf)$_2$] was investigated in water and in deuterium oxide (Figure 10). The CV experiments were performed in 10 mM phosphate buffer at pH 6.8. Under the experimental conditions used, a KIE ~ 10 was found, which suggests that a proton-coupled event is involved in the rds (Figure 10a). Using α-[Fe(mcp)(Cl)$_2$]Cl in a 0.1 M H_2SO_4 solution of pH 1, a KIE of 1 was found, which points to a different rds under acidic conditions (Figure 10b). When chemical oxidants are used to drive WO, both in neutral media ($NaIO_4$, see Table S1) and in acidic media[25] (CAN), a KIE of 1 was found. Additional details about the calculations of the KIE values are available in the Supporting Information.

Manganese Catalysts. Manganese complexes bearing tetradentate aminopyridine ligands chemically closely related to mcp have recently been described as WO electrocatalysts.[58] In addition, α-[Mn(mcp)(OTf)$_2$] and α-[Fe(mcp)(OTf)$_2$] are known to exhibit similar catalytic activity and selectivity in the oxidation of organic substrates, and their mechanisms are proposed to be virtually identical.[59−66] These precedents let us to explore the electrocatalytic water oxidation activity of α-[Mn(mcp)(OTf)$_2$]. The manganese complex was investigated electrochemically under the same conditions as α-[Fe(mcp)(OTf)$_2$] and with the same working electrodes (Figure S12). Experiments showed a common trend: in the forward scan of the CV experiments with α-[Mn(mcp)(OTf)$_2$], two oxidation events were observed between 1.1 V and 1.5 V, whereas in the backward scan, a reduction event was observed around 1.2 V (Figure 11a). This behavior can be related to the formation of a catalytically active heterogeneous species on the surface of the working electrode (Figure 11a). In order to detect any possible deposition of material on the electrode surface, after a regular CV the electrode was taken out of the solution containing the manganese catalyst, rinsed with Milli-Q water, and placed in a cell containing the electrolyte solution without any complex present. A CV was then measured and compared to a blank measurement of the same electrode, previously measured under the same conditions, in the absence of the complex. Figure 11b shows clear signs of a deposition of a catalytically active material present on the surface of the working electrode. In contrast, no signs of deposition are observed if the same experiment is carried out in the case of α-[Fe(mcp)(OTf)$_2$] (Figure S13).

In order to further investigate the formation of any surface deposit, electrochemical quartz crystal microbalance (EQCM) experiments were carried out.[49,50] Figure 12a shows the results of an EQCM experiment with α-[Mn(mcp)(OTf)$_2$]. A decrease of the catalytic current over the first 25 scans was observed simultaneously with a decrease in the resonance frequency. The decrease in frequency was already present in the first scan and became consistent in the further scans. This behavior indicates a mass deposition, probably manganese oxide,[67] on the electrode surface.

Microbalance studies in chronoamperometry mode were performed, by applying a potential of 2.0 V for 10 min while monitoring the change in the resonance frequency. The value of the resonance frequency of the quartz crystal shows a linear decay over time, indicating a constant mass deposition on the electrode surface (Figure 12b). Mass deposition was observed

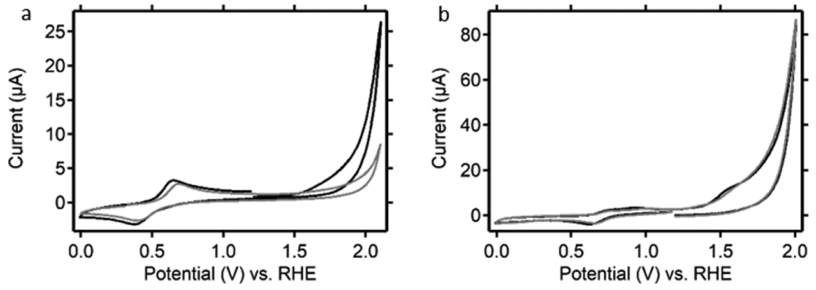

Figure 10. (a) Results of CV experiments of α-[Fe(mcp)(OTf)$_2$] (1 mM) using a GC working electrode, at a scan rate of 20 mV/s. The experiments were performed in 10 mM phosphate buffer solution at pH 6.8 with 0.1 M Na_2SO_4 to maintain the ionic strength. The figure displays the first scans of the experiments performed in water (black) and in deuterium oxide (gray). (b) Results of CV experiments of α-[Fe(mcp)(Cl)$_2$]Cl (1 mM) using a GC working electrode, at a scan rate of 20 mV/s. The experiments were performed in 0.1 M H_2SO_4 at pH 1. The figure shows the first scans of the experiments performed in water (black) and in deuterium oxide (gray).

https://dx.doi.org/10.1021/acscatal.0c05439
ACS Catal. 2021, 11, 2583−2595

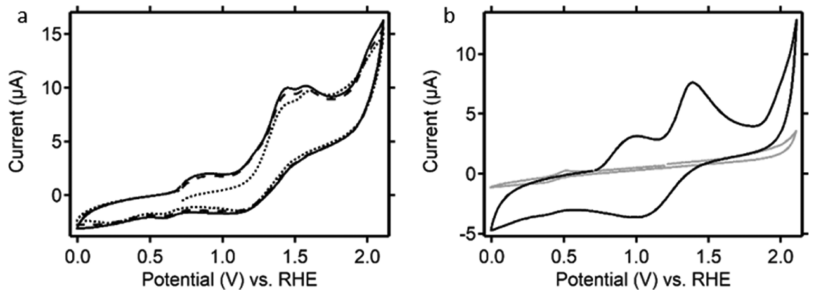

Figure 11. CV of 1 mM α-[Mn(mcp)$(OTf)_2$] (a) in 0.1 M Na_2SO_4, at a scan rate of 20 mV/s, using a BDD working electrode. Shown are the first (dotted line), second (dashed line), and third scans (solid line). (b) CV of a BDD working electrode in 0.1 M Na_2SO_4 blank solution at a scan rate of 20 mV/s, recorded before (gray) and after (black) the CV shown in (a).

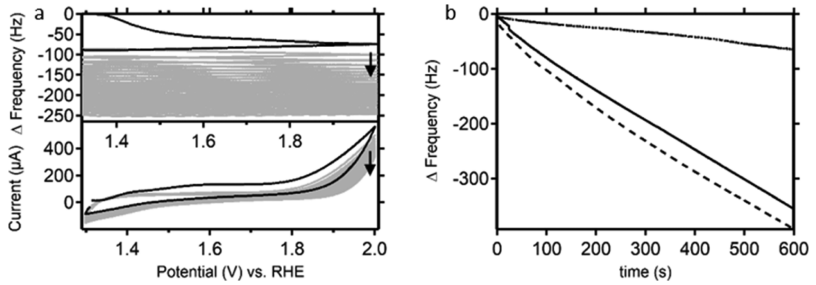

Figure 12. (a) CV in combination with EQCM of α-[Mn(mcp)$(OTf)_2$] (1 mM) in 0.1 M Na_2SO_4 at a scan rate of 100 mV/s, using a gold working electrode. Shown are scan 1 (black) and scans 2 to 25 (gray) of the CV experiment (bottom) and the corresponding change in resonance frequency (top). (b) Chronoamperometry in combination with EQCM of α-[Mn(mcp)$(OTf)_2$] (1 mM) in 0.1 M Na_2SO_4, using a gold working electrode, keeping the potential at 2.0 V vs RHE for 10 min (solid line), at 1.5 V vs RHE for 10 min (dashed line) and at 1.3 V vs RHE for 10 min (dotted line).

also at lower potential values. Therefore, a chronoamperometry experiment was performed at 1.5 V versus RHE for 2 h in order to first produce a thick manganese oxide layer on top of the gold electrode. After this experiment, the electrode was placed in a blank electrolyte solution to perform an OLEMS experiment, which confirmed that the deposit indeed produces large amounts of dioxygen (Figure 13). No traces of carbon dioxide were detected in the process, which suggests that active manganese sites are mainly produced at the top of a relative thick oxide layer. All evidence points to the conclusion that in the case of α-[Mn(mcp)$(OTf)_2$], the catalytic process takes place on the electrode surface because of the formation of a manganese oxide layer, which is active toward WO.[67−71] There is no sign of a catalytic reaction taking place in solution. We conclude that even though the Fe(mcp) and Mn(mcp) complexes are very similar in structure, their behavior under catalytic water oxidation conditions is largely different, which is most likely because of manganese(II) ions being notoriously labile.

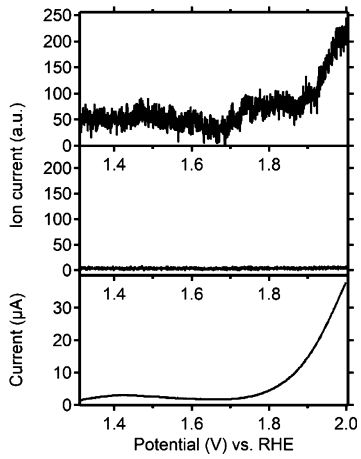

Figure 13. CV in combination with OLEMS of a gold working electrode covered by a MnO layer, recorded in 0.1 M Na_2SO_4 at a scan rate of 1 mV/s. Depicted are the m/z traces of O_2 (top), CO_2 (middle), and the corresponding current (bottom). For the sake of clarity, only the forward sweep of the second scan is shown. The MnO layer was produced during a chronoamperometry experiment while keeping the potential at 1.5 V for 2 h.

DISCUSSION

CV of α-[Fe(mcp)$(OTf)_2$] in aqueous $NaClO_4$ (0.1 M) and Na_2SO_4 (0.1 M) electrolyte solutions shows an irreversible oxidation wave starting at about 1.7 V associated with water oxidation. The same wave is observed when using a glassy carbon (GC) electrode, a basal plane pyrolytic graphite (PG) electrode, a boron-doped diamond (BDD) electrode, and a gold electrode. Online electrochemical mass spectrometry (OLEMS) experiments show that the electrochemical wave correlates with the generation of O_2, demonstrating that it corresponds to an electrocatalytic water oxidation wave. In the case of PG electrodes, water oxidation occurs in combination with oxidation of the electrode, producing CO_2. However, with noncarbonaceous electrodes, CO_2 formation is not observed, suggesting that it is not produced by oxidation of the ligand of the catalyst but rather by oxidation of the carbon-based electrode material. Thus, the data strongly suggest that catalytic water oxidation is performed by the intact catalyst. In addition, electrochemical quartz crystal microbalance (EQCM) experiments show that there is no deposition of

https://dx.doi.org/10.1021/acscatal.0c05439
ACS Catal. 2021, 11, 2583−2595

(catalytically active) material on the electrode, strongly suggesting that the catalytic water oxidation takes place in the homogeneous phase.

In terms of molecular nature and catalytic current, the performance of the Fe(mcp) systems is similar to that of the dinuclear iron catalyst [(MeOH)Fe(Hbbpya)−μ−O−(Hbbpya)Fe(MeOH)](OTf)$_4$.[33] Moreover, both complexes showed an overpotential in the range of 300−500 mV with respect to the thermodynamic water oxidation potential of 1.23 V. In terms of TOF the Fe(mcp) systems showed a value of 0.41 s^{-1} in the presence of chemical oxidants[25,37,38] and the Fe(Hbbpya) system showed a value of 0.12 s^{-1} under electrochemical conditions. .[33] The advantage of the Fe(mcp) system is that it was proved to be active under both neutral and acidic pH conditions, providing that one starts with a +III precursor, whereas [(MeOH)Fe(Hbbpya)−μ−O−(Hbbpya)-Fe(MeOH)](OTf)$_4$ did not show stability at pH 1. It should be mentioned though that α-[Fe(mcp)(OTf)$_2$] showed good catalytic rates at low pH in the presence of cerium(IV) ammonium nitrate (CAN), but the electrochemical studies of α-[Fe(mcp)(OTf)$_2$] under such low pH conditions were excluded because of the demetallation of the iron(II) precursor, which occurs on the time scale required for the electrochemical experiment. In the presence of CAN, the iron(II) precursor is instantaneously oxidized to the iron(III) species, which is stable against hydrolysis. Following a rational design, the iron(III) complex α-[Fe(mcp)(Cl)$_2$]Cl was proved to be stable and active in the acidic electrolyte (pH 1, 0.1 M H_2SO_4). The TOF values found with our catalysts are still low when compared to the pentanuclear iron catalyst reported by Masaoka *et al.*, with a TOF = 1900 s^{-1}.[32] However, the pentanuclear system operated at an overpotential higher than 500 mV and in an acetonitrile/water mixture. Therefore, our Fe(mcp) water oxidation catalysts offer the advantages of stability and activity at neutral and acidic pH values, a lower overpotential compared to some of the benchmark systems, including Fe(dpaq),[26] Fe(cyclam),[31] Fe(bbpya),[33] and other tetradentate polypyridyl type ligands,[29] and the ability to operate in aqueous solutions (dpaq = 2-[bis(pyridine-2-ylmethyl)]amino-*N*-quinolin-8-yl-acetamido and bbpya = *N*,*N*-bis(2,2′-bipyrid-6-yl)amine).

However, in contrast to the results obtained for the iron catalysts reported in this study, the manganese catalyst α-[Mn(mcp)(OTf)$_2$] exhibits signs of complex degradation and deposition of manganese oxide on the electrode, which is responsible for the observed catalytic activity.

Overall, the reaction rates for electrocatalytic water oxidation in the presence of the Fe(mcp) systems are modest, with an overpotential on the scale of approximately 500 mV with respect to the thermodynamic potential of the water oxidation reaction of 1.23 V, suggesting the existence of kinetic barriers for the reaction. In this regard, previous work has shown that Fe^{III}/Fe^{IV} oxidation on related complexes entails a slow $Fe^{III}(OH)/Fe^{IV}(O)$ proton-coupled electron transfer associated with relatively large reorganization energy values, which presumably arise from a spin-state barrier.[72]

Most notably, our mechanistic analyses indicate that the electrocatalytic reaction is first order in the iron catalyst and that the rds has a large KIE ∼ 10 at neutral pH.

In order to understand the origin of this large KIE, it should be considered that under electrocatalytic conditions, the water oxidation onset potential can be ascribed to the formation of the catalytically active species. In the case of α-[Fe(mcp)-(OTf)$_2$], the onset potential was found at about 1.7 V versus RHE under electrochemical conditions (pH 5). This value correlates well with the previously calculated redox potentials of the Fe^V/Fe^{IV} redox couple for the α-[Fe(mep)(OTf)$_2$] complex (mep = *N*,*N*′-dimethyl-*N*,*N*′-bis(2-pyridylmethyl)-ethylenediamine). A redox potential value of 1.73 V versus NHE was found for the $Fe^{IV}(O)(OH_2)$ to $Fe^V(O)(OH)$ transition (computed at pH 1).[73] In addition, previous studies determined that $Fe^{IV}(O)(OH_2)$ species in related nonheme complexes were not able to form the O−O bond required for oxygen evolution.[74] Therefore, it is reasonable to suggest that the onset of the electrocatalytic wave may correspond to the formation of $Fe^V(O)(OH)$ from $Fe^{IV}(O)(OH_2)$ species, and is the rds.

When comparing the catalytic mechanism between electrochemical conditions and chemical oxidant-driven conditions for Fe(mcp) and related complexes, clear differences between the two regimes become apparent. These differences are most notable when comparing the KIE values obtained under electrocatalytic conditions to KIE values obtained when water oxidation is driven by chemical oxidants. The [Fe-(OTf)$_2$(pytacn)] (pytacn = 1-(2-pyridylmethyl)-4,7-dimethyl-1,4,7-triazacyclononane) catalyst has been shown to perform WO with a KIE of approximately 1 when using $NaIO_4$ and CAN, compared to a KIE of 10 under electrocatalytic conditions.[25] In order to determine whether these differences in KIE arise from the different nature of the catalyst or by the type of terminal oxidant (electrocatalysis vs chemical oxidants), we have evaluated the KIE for the α-[Fe(mcp)-(OTf)$_2$] complex when using chemical oxidants. Turnover frequencies were determined by manometry and are collected in Table S1 in the Supporting Information. When using CAN, which operates at low pH (pH = 0.8), we have found that the KIE is ca. 1.0, which matches well with the electrochemistry experiments under acidic conditions. Considering that a KIE of 10 was obtained electrochemically at higher pH values, we have also evaluated the KIE at different pH values ranging from 4.6 to 10, using $NaIO_4$ as the oxidant (see Table S1). Again, under these conditions, a KIE of approximately 1 is observed. Therefore, chemical and electrochemical water oxidation conducted at neutral pH values exhibits different KIE values indicating that they have different rds.

Previous studies have addressed the mechanism of water oxidation performed with the catalysts studied in this work in the presence of chemical oxidants.[37,41,73] In the particular case of α-[Fe(mcp)(OTf)$_2$], mechanistic studies under acidic conditions using Ce^{IV} as a sacrificial oxidant, aided by spectroscopic analysis, have identified the high-valent intermediate $Fe^{IV}(O)(OH_2)$ as the resting state at a low concentration of Ce^{IV}. This species undergoes a one electron oxidation to form $Fe^V(O)(OH)$ via an inner sphere electron transfer process that proceeds through a heterometallic Fe^{IV}−O−Ce^{IV} species. The latter accumulates when large concentrations of Ce^{IV} are used, enabling mass spectrometric and spectroscopic characterization.[37] The heterometallic Fe^{IV}−O−Ce^{IV} species constitutes the last detectable intermediate of the catalytic cycle prior to dioxygen formation and its evolution toward the reactive $Fe^V(O)(OH)$ species via internal electron transfer presumably constitutes the rds of the reaction. Computational analysis indicates that attack of the water molecule on $Fe^V(O)(OH)$ is initially assisted by an interaction with the hydroxide ligand at the same iron center.[73] Proton-coupled electron transfer from the incoming water molecule to

https://dx.doi.org/10.1021/acscatal.0c05439
ACS Catal. 2021, 11, 2583−2595

$Fe^{V}(O)(OH)$ forms an $\{Fe^{IV}(O)(OH_2)\cdot OH\}$ intermediate from which the O−O bond is rapidly formed. The reaction of $Fe^{V}(O)(OH)$ with the water molecule must be fast and takes place after the rds, accounting for the lack of an isotope effect.

The large KIE values obtained with the electrocatalytic WO at pH 7 require an alternative explanation. Large KIE values in water oxidation reactions are uncommon, but several notable precedents have been reported. Electrochemical studies of Meyer *et al.* on $[Ru(Mebimpy)(bpy)(OH_2)]^{2+}$ (Mebimpy = 2,6-bis(1-methylbenzylimidazol-2-yl)pyridine complexes) revealed a KIE value ranging from 6.6 in pure water to 2.3 in the presence of HPO_4^{2-} as the base, suggesting that added bases accelerate the O−O bond formation by concerted atom-proton transfer (ATP). Higher reaction rates were observed with conjugated bases with a higher pK_a value.[7] Another example of a large KIE (20) under electrocatalytic conditions was found for the water oxidation catalyst $\{[(Me_2TMPA)\text{-}Cu^{II}]_2\text{-}(\mu\text{-}OH)_2\}(OTf)_2$ (Me_2TMPA = bis((6-methyl-2-pyridyl)methyl)(2-pyridylmethyl)-amine). In this case, a PCET step ($\{Cu^{II}(\mu\text{-}OH)_2Cu^{II}\} \rightarrow \{Cu^{II}(\mu\text{-}OH)(\mu\text{-}O)Cu^{III}\} + e^- + H^+$) is considered to be responsible for the large kinetic barrier.[75]

Therefore, the large KIE value of 10 that we observe under electrocatalytic conditions at neutral pH is reminiscent of the PCET process observed in the high-valent copper active species, and may indicate that PCET from the $Fe^{IV}(O)(OH_2)$ to $Fe^{V}(O)(OH)$ takes place during the rds.

CONCLUSIONS

The electrochemical experiments performed on the Fe(mcp) systems under acidic conditions showed that the results obtained with chemical oxidants can largely be reproduced electrochemically. Furthermore, it was proven that these systems are electrocatalytically active toward water oxidation under pH-neutral conditions, which are more suitable for applications compared to strongly acidic conditions. The evolution of dioxygen was proven with OLEMS experiments and no CO_2 formation originating from the organic ligands was detected, confirming the stability of the catalysts. Moreover, these catalysts were proved to be molecular systems, as confirmed by EQCM experiments where no formation of deposits on the working electrodes was observed. A counter-check of the molecularity of the systems was obtained by studying the manganese catalyst α-$[Mn(mcp)(OTf)_2]$, for which a heterogeneous species formed at the surface of the working electrode is instead responsible for the catalytic activity. Apart from the manganese system, all the complexes studied showed comparable activity toward the water oxidation reaction. By studying various structural analogues of the Fe(mcp)-complex, the stability of the catalytic system under electrochemical conditions was confirmed. The mechanistic studies provided more insights into the catalytic mechanism, showing that the reaction proceeds with a different rds with respect to what was previously proposed when using chemical oxidants.[25,38] This reflects the significance of detailed electrocatalytic studies in addition to the use of chemical oxidants, which take active part in the reaction mechanism. As shown in previous studies, the reaction of the iron complex with Ce^{IV} generates a Fe^{IV}−O−Ce^{IV} complex, which acts as an inner-sphere electron transfer intermediate, leading to the 1 e^- oxidation of the iron center, which later undergoes a water nucleophilic attack.[38] Overall, the findings of this study highlight the importance of the electrochemical studies to evaluate water oxidation catalysts.

EXPERIMENTAL SECTION

The reagents and solvents used were commercially available and purchased from Panreac, Scharlau, and Aldrich. Preparation and handling of air-sensitive materials were carried out in a N_2 glovebox (MBraun ULK 1000) with O_2 and H_2O concentrations < 5 ppm. Cerium(IV) ammonium nitrate (CAN) ≥99.5% trace metals basis were purchased from Sigma-Aldrich. Water (18.2 MΩ cm) was purified with a Milli-Q Millipore Gradient AIS system. D_2O was purchased and directly used from Sigma Aldrich. The complexes α-$[Fe(mcp)(OTf)_2]$, α-$[Fe(D4\text{-}mcp)(OTf)_2]$, α-$[Fe(mcp)(Cl)_2]Cl$, β-$[Fe(mcp)(OTf)_2]$, and α-$[Mn(mcp)(OTf)_2]$ were synthesized and characterized according to previous procedures[38,59,60] and except for the iron(III) complex stored in an argon-filled glovebox to prevent oxidation in air.

Electrochemical Experiments. All electrochemical measurements with the exception of the EQCM experiments (details below) were performed in a custom-made single-compartment glass cell using a three-electrode setup. In all cases, the data were recorded either on an Ivium potentiostat, operated by IviumSoft software, or on an Autolab PGstat10 potentiostat operated by NOVA 2.1.2 software. The working electrodes used in the experiments were a pyrolytic graphite (PG) disk with a (geometric) surface area of 0.20 cm^2, two gold disks with a (geometric) surface area of 0.13 cm^2 and 0.18 cm^2, a glassy-carbon (GC) rod with a surface area of 0.07 cm^2, a boron-doped-diamond (BDD) disk with a surface area of 0.07 cm^2, and indium tin oxide (ITO)-coated glass plates. A large surface area gold plate was used as a counter electrode. The reference electrode was a reversible hydrogen electrode (RHE) made up of a platinum mesh in the H_2-saturated electrolyte at the same pH as the working solution. The cell and the reference electrode were connected via a Luggin capillary.

The gold electrode was prepared before each experiment by oxidizing the surface at 10 V for 30 s in a 10% H_2SO_4 solution, followed by stripping of the gold oxide layer in 6 M HCl solution and subsequent electropolishing of the electrode by scanning for 200 cycles between 0.0 and 1.75 V versus RHE at 1 V/s in 0.1 M $HClO_4$ electrolyte solution.

A fresh PG surface was prepared before each experiment by polishing the working electrode with sandpaper and subsequently removing excess debris by sonication in Milli-Q water for at least 5 min.

For the experiments with an ITO working electrode, a small slice of ITO-covered glass (ca. 0.5·1.5 cm) was used. While the gold and PG working electrodes were used in the hanging meniscus configuration, the ITO electrode was partially submerged in the electrolyte solution.

The GC electrode was pretreated before each experiment by polishing the electrode surface with alumina suspensions (1.0 μm followed by 0.3 μm and 0.05 μm). The polishing was followed by removing the excess debris by sonicating the electrode in Milli-Q water for 10 min.

The BDD electrode was prepared by sonication for 5 min in Milli-Q water. Subsequently, the electrode was electropolished by scanning 200 cycles between −1.0 and 2.25 V versus RHE at 1 V/s in 0.1 M H_2SO_4 solution.

All glassware used in the electrochemical measurements was routinely cleaned of any organic contamination overnight with

https://dx.doi.org/10.1021/acscatal.0c05439
ACS Catal. 2021, 11, 2583−2595

0.5 M H_2SO_4 solution containing 1 g/L $KMnO_4$. The metal particles were afterward removed by cleaning the glassware for 30 min with Milli-Q grade water (>18.2 MΩ cm resistivity) containing a few droplets of concentrated H_2SO_4 and 35% H_2O_2. The glassware was then cleaned by threefold rinsing with Milli-Q grade water and boiling it in Milli-Q grade water.

The electrolyte solutions were prepared from p.a. grade chemicals obtained from Merck (Suprapur) and Milli-Q water (resistivity >18.2 MΩ cm). The phosphate buffer solutions (10 mM) were prepared by using NaH_2PO_4 and Na_2HPO_4 with the addition of Na_2SO_4 (0.1 M) to maintain the ionic strength.

Prior to measurements, the electrolyte solution was purged of air by bubbling with argon (Linde, Ar 5.0) for at least 20 min. During the measurements, the cell was constantly kept under argon flow to prevent air from entering.

For the OLEMS measurements, the gases formed at the working electrode were collected via a hydrophobic tip (KEL-F with a porous Teflon plug) in close proximity to the surface of the working electrode and analyzed using a QMS 200 mass spectrometer. A detailed description of the OLEMS setup is available elsewhere.[53] All electrochemical potential cycling in combination with OLEMS was done at a scan rate of 1 mV/s.

EQCM experiments were performed in a 3 mL Teflon cell purchased from Autolab. The top part of the cell was modified to allow for electrochemical measurements under an inert atmosphere. The EQCM was controlled using an Autolab potentiostat operated by NOVA 2.0 software. Autolab EQCM electrodes with a surface area of 1.5 cm^2 consisting of a 200 nm gold layer deposited on a quartz crystal were used as working electrodes. A custom-made RHE reference electrode was used, which is described elsewhere.[54]

Online analysis of the gas mixture during long-term chronoamperometry to determine the FY was performed using a NeoFox oxygen-sensing system equipped with a FOSFOR-R probe. A tight three-electrode electrochemical cell was filled with 15 mL of the electrolyte solution (10 mM phosphate buffer at pH 6.8) and, after sealing, a constant flow of Ar gas (40 mL/min) was applied, with the O_2 sensor probe placed in the headspace of the cell. Meanwhile, ca. 11 mg of the α-[Fe(mcp)$(OTf)_2$] complex was weighed and kept under an inert atmosphere until the electrolyte solution became O_2-free. At this point, about 2 mL of this solution was withdrawn from the cell and used to dissolve the catalyst powder. Once the catalyst stock solution was prepared, it was rapidly injected in the electrochemical cell. The final concentration was 1.1 mM in 15 mL of the electrolyte. To perform the experiment, the cell was equipped with the FTO-covered glass slide (1 × 2.5 cm^2) as the working electrode, a SCE reference electrode, and a Pt wire as the counter electrode. Chronoamperometry was run at a constant potential of 1.65 V versus RHE for 30 min.

The volume (in μL) of O_2 evolved was determined using the following equation

$$V_{O_2} = \frac{p_M}{p} V_{HS} \cdot 10^6$$

where p_M is the measured O_2 pressure (in torr), p is the ambient pressure (760 torr), V_{HS} is the volume of the headspace, and the factor 10^6 is used to convert the volume in μL. To obtain the FY, the V_{O_2} value is divided by theoretical amount of O_2 produced, based on the chronoamperometry, as follows

$$FY = \frac{V_{O_2}}{V_{O_2}(th)} * 100$$

where

$$V_{O_2}(th) = \frac{i*t}{4} \cdot \frac{RT}{F} \cdot 10^6$$

$V_{O_2}(th)$ is the theoretical amount of O_2 in μL, i is the current passed, t is the time, factor 4 accounts for the stoichiometric in WO, R is the gas constant (0.0821 L atm mol^{-1} K^{-1}), T is the temperature (298 K), and F is the Faraday constant (96,485 C mol^{-1}).

Sample Preparation. Samples of complexes α-[Fe(mcp)$(OTf)_2$], α-[Fe(D4-mcp)$(OTf)_2$], β-[Fe(mcp)$(OTf)_2$], and α-[Mn(mcp)$(OTf)_2$] were weighed in an argon atmosphere inside the glovebox and stored in a closed vessel. Prior to the experiment, the complexes were dissolved in a small amount of electrolyte solution (typically 1−2 mL) taken from the cell, which had previously been purged with argon and subsequently added to the electrochemical cell. The electrolyte solution was then purged again by bubbling with argon for several minutes.

Samples of complex α-[Fe(mcp)$(Cl)_2$]Cl were weighed in air and subsequently added to the cell in a manner analogous to that described for the iron(II) complexes.

For the electrochemical experiments, 1.0 mM and 1.1 mM concentrations of the catalyst were used.

General Procedure for the Chemically Driven WO Reactions. In a crimped 20 mL vial, CAN (685.29 mg, 1000 equiv, final concentration = 125 mM) was dissolved in Milli-Q water (9.5 mL) at room temperature leading to an orange solution. The headspace of the vial containing the resulting solution was monitored with an atmospheric pressure sensor transducer. After equilibration of the pressure signal, iron complex α-[Fe(mcp)$(OTf)_2$] (0.5 mL of a stock solution of 2 mg in 11.8 mL Milli-Q water, final concentration = 12.5 μM) was added and the evolved gas was monitored along the reaction time. Then, an aliquot of the headspace (150 μL) was analyzed in the GC-TCD to quantify the O_2 and CO_2 present in the headspace.

■ ASSOCIATED CONTENT

Supporting Information

The Supporting Information is available free of charge at https://pubs.acs.org/doi/10.1021/acscatal.0c05439.

The CV of α-[Fe(mcp)$(OTf)_2$] with different working electrodes; UV−vis stability tests on [α-Fe(mcp)$(OTf)_2$] and on α-[Fe(mcp)$(Cl)_2$]Cl; CV of α-[Fe(mcp)$(Cl)_2$]Cl, OLEMS of α-[Fe(mcp)$(Cl)_2$]Cl, and OLEMS of α-[Fe(D4-mcp)$OTf)_2$]; mechanistic studies; and CV of α-[Mn(mcp)$(OTf)_2$] with different working electrodes (PDF)

■ AUTHOR INFORMATION

Corresponding Authors

Miquel Costas − *Institut de Química Computacional i Catàlisi (IQCC) and Departament de Química, Universitat de Girona, 17003 Girona, Spain;* orcid.org/0000-0001-6326-8299; Email: miquel.costas@udg.edu

Julio Lloret-Fillol − *Institute of Chemical Research of Catalonia, Spain (ICIQ), The Barcelona Institute of Science and Technology, 43007 Tarragona, Spain; Catalan*

https://dx.doi.org/10.1021/acscatal.0c05439
ACS Catal. 2021, 11, 2583−2595

*Institution for Research and Advanced Studies (ICREA), 08010 Barcelona, Spain; orcid.org/0000-0002-4240-9512; Email: jlloret@iciq.es

Dennis G.H. Hetterscheid − *Leiden Institute of Chemistry, Leiden University, 2300 RA Leiden, The Netherlands; orcid.org/0000-0001-5640-4416; Email: d.g.h.hetterscheid@chem.leidenuniv.nl

Authors

Silvia D'Agostini − *Leiden Institute of Chemistry, Leiden University, 2300 RA Leiden, The Netherlands*

Konstantin G. Kottrup − *Leiden Institute of Chemistry, Leiden University, 2300 RA Leiden, The Netherlands*

Carla Casadevall − *Institute of Chemical Research of Catalonia, Spain (ICIQ), The Barcelona Institute of Science and Technology, 43007 Tarragona, Spain; orcid.org/0000-0002-3090-4938*

Ilaria Gamba − *Institut de Química Computacional i Catàlisi (IQCC) and Departament de Química, Universitat de Girona, 17003 Girona, Spain*

Valeria Dantignana − *Institut de Química Computacional i Catàlisi (IQCC) and Departament de Química, Universitat de Girona, 17003 Girona, Spain*

Alberto Bucci − *Institute of Chemical Research of Catalonia, Spain (ICIQ), The Barcelona Institute of Science and Technology, 43007 Tarragona, Spain*

Complete contact information is available at: https://pubs.acs.org/10.1021/acscatal.0c05439

Author Contributions

S.D. and K.G.K. contributed equally. This article was written through contributions of all authors. All authors have given approval to the final version of the manuscript.

Funding

NWO Echo grant 717.014.008. PGC2018-101737-B-I00 and 2017 SGR 00264 grants.

Notes

The authors declare no competing financial interest.

■ ACKNOWLEDGMENTS

The Netherlands' Organization for Scientific Research (NWO) is acknowledged for financial support (Echo grant 717.014.008). We acknowledge the support of the Spanish Ministry of Science, Innovation, and Universities (PGC2018-101737-B-I00) to M.C. and the Generalitat de Catalunya (2017 SGR 00264 and ICREA Academia). Thanks to MINECO FPU14/02550 (C.C.), ICIQ Foundation, ERC for project FP7-PEOPLE-2010-ERG-268445 (J.L.F.), and CELLEX Foundation (CELLEX-ICIQ high-throughput platform).

■ REFERENCES

(1) Lewis, N. S.; Nocera, D. G. Powering the planet: Chemical challenges in solar energy utilization. *Proc. Natl. Acad. Sci. U. S. A* **2006**, *103*, 15729−15735.

(2) de Ruiter, J. M.; Monti, A.; van der Ham, C. J. M.; Gullo, M. P.; Joya, K. S.; D'Angelantonio, M.; Barbieri, A.; Hetterscheid, D. G. H.; de Groot, H. J. M.; Buda, F.; Buda, F. Electrochemical and Spectroscopic Study of Mononuclear Ruthenium Water Oxidation Catalysts: A Combined Experimental and Theoretical Investigation. *ACS Catal.* **2016**, *6*, 7340−7349.

(3) Duan, L.; Bozoglian, F.; Mandal, S.; Stewart, B.; Privalov, T.; Llobet, A.; Sun, L. A molecular ruthenium catalyst with water-oxidation activity comparable to that of photosystem II. *Nat. Chem.* **2012**, *4*, 418−423.

(4) Duan, L.; Wang, L.; Li, F.; Li, F.; Sun, L. Highly Efficient Bioinspired Molecular Ru Water Oxidation Catalysts with Negatively Charged Backbone Ligands. *Acc. Chem. Res.* **2015**, *48*, 2084−2096.

(5) Matheu, R.; Ertem, M. Z.; Benet-Buchholz, J.; Coronado, E.; Batista, V. S.; Sala, X.; Llobet, A. Intramolecular Proton Transfer Boosts Water Oxidation Catalyzed by a Ru Complex. *J. Am. Chem. Soc.* **2015**, *137*, 10786−10795.

(6) Wang, L.; Duan, L.; Wang, Y.; Ahlquist, M. S. G.; Sun, L. Highly efficient and robust molecular water oxidation catalysts based on ruthenium complexes. *Chem. Commun.* **2014**, *50*, 12947−12950.

(7) Chen, Z.; Concepcion, J. J.; Hu, X.; Yang, W.; Hoertz, P. G.; Meyer, T. J. Concerted O atom−proton transfer in the O—O bond forming step in water oxidation. *Proc. Natl. Acad. Sci. U. S. A* **2010**, *107*, 7225−7229.

(8) Concepcion, J. J.; Jurss, J. W.; Hoertz, P. G.; Meyer, T. J. Catalytic and Surface-Electrocatalytic Water Oxidation by Redox Mediator−Catalyst Assemblies. *Angew. Chem., Int. Ed.* **2009**, *48*, 9473−9476.

(9) Meyer, T. J.; Sheridan, M. V.; Sherman, B. D. Mechanisms of molecular water oxidation in solution and on oxide surfaces. *Chem. Soc. Rev.* **2017**, *46*, 6148−6169.

(10) Vannucci, A. K.; Alibabaei, L.; Losego, M. D.; Concepcion, J. J.; Kalanyan, B.; Parsons, G. N.; Meyer, T. J. Crossing the divide between homogeneous and heterogeneous catalysis in water oxidation. *Proc. Natl. Acad. Sci. U. S. A* **2013**, *110*, 20918−20922.

(11) Gersten, S. W.; Samuels, G. J.; Meyer, T. J. Catalytic oxidation of water by an oxo-bridged ruthenium dimer. *J. Am. Chem. Soc.* **1982**, *104*, 4029−4030.

(12) Bucci, A.; Savini, A.; Rocchigiani, L.; Zuccaccia, C.; Rizzato, S.; Albinati, A.; Llobet, A.; Macchioni, A. Organometallic Iridium Catalysts Based on Pyridinecarboxylate Ligands for the Oxidative Splitting of Water. *Organometallics* **2012**, *31*, 8071−8074.

(13) Diaz-Morales, O.; Hersbach, T. J. P.; Hetterscheid, D. G. H.; Reek, J. N. H.; Koper, M. T. M. Electrochemical and Spectroelectrochemical Characterization of an Iridium-Based Molecular Catalyst for Water Splitting: Turnover Frequencies, Stability, and Electrolyte Effects. *J. Am. Chem. Soc.* **2014**, *136*, 10432−10439.

(14) Menendez Rodriguez, G.; Bucci, A.; Hutchinson, R.; Bellachioma, G.; Zuccaccia, C.; Giovagnoli, S.; Idriss, H.; Macchioni, A. Extremely Active, Tunable, and pH-Responsive Iridium Water Oxidation Catalysts. *ACS Energy Lett.* **2017**, *2*, 105−110.

(15) Blakemore, J. D.; Schley, N. D.; Olack, G. W.; Incarvito, C. D.; Brudvig, G. W.; Crabtree, R. H. Anodic deposition of a robust iridium-based water-oxidation catalyst from organometallic precursors. *Chem. Sci.* **2011**, *2*, 94−98.

(16) Blakemore, J. D.; Mara, M. W.; Kushner-Lenhoff, M. N.; Schley, N. D.; Konezny, S. J.; Rivalta, I.; Negre, C. F. A.; Snoeberger, R. C.; Kokhan, O.; Huang, J.; Stickrath, A.; Tran, L. A.; Parr, M. L.; Chen, L. X.; Tiede, D. M.; Batista, V. S.; Crabtree, R. H.; Brudvig, G. W. Characterization of an Amorphous Iridium Water-Oxidation Catalyst Electrodeposited from Organometallic Precursors. *Inorg. Chem.* **2013**, *52*, 1860−1871.

(17) Hintermair, U.; Sheehan, S. W.; Parent, A. R.; Ess, D. H.; Richens, D. T.; Vaccaro, P. H.; Brudvig, G. W.; Crabtree, R. H. Precursor Transformation during Molecular Oxidation Catalysis with Organometallic Iridium Complexes. *J. Am. Chem. Soc.* **2013**, *135*, 10837−10851.

(18) Huang, J.; Blakemore, J. D.; Fazi, D.; Kokhan, O.; Schley, N. D.; Crabtree, R. H.; Brudvig, G. W.; Tiede, D. M. Domain structure for an amorphous iridium-oxide water-oxidation catalyst characterized by X-ray pair distribution function analysis. *Phys. Chem. Chem. Phys.* **2014**, *16*, 1814−1819.

(19) Creus, J.; Matheu, R.; Peñafiel, I.; Moonshiram, D.; Blondeau, P.; Benet-Buchholz, J.; García-Antón, J.; Sala, X.; Godard, C.; Llobet, A. A Million Turnover Molecular Anode for Catalytic Water Oxidation. *Angew. Chem., Int. Ed.* **2016**, *55*, 15382−15386.

(20) Tamaki, Y.; Vannucci, A. K.; Dares, C. J.; Binstead, R. A.; Meyer, T. J. One-Electron Activation of Water Oxidation Catalysis. *J. Am. Chem. Soc.* **2014**, *136*, 6854−6857.
(21) Sheehan, S. W.; Thomsen, J. M.; Hintermair, U.; Crabtree, R. H.; Brudvig, G. W.; Schmuttenmaer, C. A. A molecular catalyst for water oxidation that binds to metal oxide surfaces. *Nat. Commun.* **2015**, *6*, 6469.
(22) Blakemore, J. D.; Crabtree, R. H.; Brudvig, G. W. Molecular Catalysts for Water Oxidation. *Chem. Rev.* **2015**, *115*, 12974−13005.
(23) Kärkäs, M. D.; Åkermark, B. Water oxidation using earth-abundant transition metal catalysts: opportunities and challenges. *Dalton Trans.* **2016**, *45*, 14421−14461.
(24) Ellis, W. C.; McDaniel, N. D.; Bernhard, S.; Collins, T. J. Fast Water Oxidation Using Iron. *J. Am. Chem. Soc.* **2010**, *132*, 10990−10991.
(25) Fillol, J. L.; Codolà, Z.; Garcia-Bosch, I.; Gómez, L.; Pla, J. J.; Costas, M. Efficient water oxidation catalysts based on readily available iron coordination complexes. *Nat. Chem.* **2011**, *3*, 807−813.
(26) Coggins, M. K.; Zhang, M.-T.; Vannucci, A. K.; Dares, C. J.; Meyer, T. J. Electrocatalytic Water Oxidation by a Monomeric Amidate-Ligated Fe(III)−Aqua Complex. *J. Am. Chem. Soc.* **2014**, *136*, 5531−5534.
(27) Zhang, B.; Li, F.; Yu, F.; Cui, H.; Zhou, X.; Li, H.; Wang, Y.; Sun, L. Homogeneous Oxidation of Water by Iron Complexes with Macrocyclic Ligands. *Chem.—Asian J.* **2014**, *9*, 1515−1518.
(28) Tan, P.; Kwong, H.-K.; Lau, T.-C. Catalytic oxidation of water and alcohols by a robust iron(III) complex bearing a cross-bridged cyclam ligand. *Chem. Commun.* **2015**, *51*, 12189−12192.
(29) Wickramasinghe, L. D.; Zhou, R.; Zong, R.; Vo, P.; Gagnon, K. J.; Thummel, R. P. Iron Complexes of Square Planar Tetradentate Polypyridyl-Type Ligands as Catalysts for Water Oxidation. *J. Am. Chem. Soc.* **2015**, *137*, 13260−13263.
(30) Das, B.; Lee, B.-L.; Karlsson, E. A.; Åkermark, T.; Shatskiy, A.; Demeshko, S.; Liao, R.-Z.; Laine, T. M.; Haukka, M.; Zeglio, E.; Abdel-Magied, A. F.; Siegbahn, P. E. M.; Meyer, F.; Kärkäs, M. D.; Johnston, E. V.; Nordlander, E.; Åkermark, B. Water oxidation catalyzed by molecular di- and nonanuclear Fe complexes: importance of a proper ligand framework. *Dalton Trans.* **2016**, *45*, 13289−13293.
(31) Kottrup, K. G.; Hetterscheid, D. G. H. Evaluation of iron-based electrocatalysts for water oxidation - an on-line mass spectrometry approach. *Chem. Commun.* **2016**, *52*, 2643−2646.
(32) Okamura, M.; Kondo, M.; Kuga, R.; Kurashige, Y.; Yanai, T.; Hayami, S.; Praneeth, V. K. K.; Yoshida, M.; Yoneda, K.; Kawata, S.; Masaoka, S. A pentanuclear iron catalyst designed for water oxidation. *Nature* **2016**, *530*, 465−468.
(33) Kottrup, K. G.; D'Agostini, S.; van Langevelde, P. H.; Hetterscheid, D. G. H.; Hetterscheid, D. G. H. Catalytic Activity of an Iron-Based Water Oxidation Catalyst: Substrate Effects of Graphitic Electrodes. *ACS Catal.* **2018**, *8*, 1052−1061.
(34) Liu, T.; Zhang, B.; Sun, L. Iron-Based Molecular Water Oxidation Catalysts: Abundant, Cheap, and Promising. *Chem.—Asian J.* **2019**, *14*, 31−43.
(35) DeNardo, M. A.; Mills, M. R.; Ryabov, A. D.; Collins, T. J. Unifying Evaluation of the Technical Performances of Iron-Tetra-amido Macrocyclic Ligand Oxidation Catalysts. *J. Am. Chem. Soc.* **2016**, *138*, 2933−2936.
(36) Casadevall, C.; Bucci, A.; Costas, M.; Lloret-Fillol, J. Water oxidation catalysis with well-defined molecular iron complexes. In *Advances in Inorganic Chemistry*; van Eldik, R., Hubbard, C. D., Eds.; Academic Press, 2019; Vol. *74*, pp 151−196.
(37) Codolà, Z.; Gómez, L.; Kleespies, S. T.; Que, L., Jr.; Costas, M.; Lloret-Fillol, J. Evidence for an oxygen evolving iron−oxo−cerium intermediate in iron-catalysed water oxidation. *Nat. Commun.* **2015**, *6*, 5865.
(38) Codolà, Z.; Gamba, I.; Acuña-Parés, F.; Casadevall, C.; Clémancey, M.; Latour, J.-M.; Luis, J. M.; Lloret-Fillol, J.; Costas, M. Design of Iron Coordination Complexes as Highly Active Homogenous Water Oxidation Catalysts by Deuteration of Oxidation-Sensitive Sites. *J. Am. Chem. Soc.* **2019**, *141*, 323−333.
(39) Yoshida, M.; Masaoka, S.; Abe, J.; Sakai, K. Catalysis of Mononuclear Aquaruthenium Complexes in Oxygen Evolution from Water: A New Radical Coupling Path using Hydroxocerium(IV) Species. *Chem.—Asian J.* **2010**, *5*, 2369−2378.
(40) Wasylenko, D. J.; Ganesamoorthy, C.; Henderson, M. A.; Berlinguette, C. P. Unraveling the Roles of the Acid Medium, Experimental Probes, and Terminal Oxidant, $(NH_4)_2[Ce(NO_3)_6]$, in the Study of a Homogeneous Water Oxidation Catalyst. *Inorg. Chem.* **2011**, *50*, 3662−3672.
(41) Codolà, Z.; Garcia-Bosch, I.; Acuña-Parés, F.; Prat, I.; Luis, J. M.; Costas, M.; Lloret-Fillol, J. Electronic Effects on Single-Site Iron Catalysts for Water Oxidation. *Chem.—Eur. J.* **2013**, *19*, 8042−8047.
(42) Hong, D.; Mandal, S.; Yamada, Y.; Lee, Y.-M.; Nam, W.; Llobet, A.; Fukuzumi, S. Water Oxidation Catalysis with Nonheme Iron Complexes under Acidic and Basic Conditions: Homogeneous or Heterogeneous? *Inorg. Chem.* **2013**, *52*, 9522−9531.
(43) Hetterscheid, D. G. H.; Reek, J. N. H. Periodate as an Oxidant for Catalytic Water Oxidation: Oxidation via Electron Transfer or O-Atom Transfer? *Eur. J. Inorg. Chem.* **2014**, 742−749.
(44) Chen, G.; Chen, L.; Ng, S.-M.; Man, W.-L.; Lau, T.-C. Chemical and visible-light-driven water oxidation by iron complexes at pH 7-9: evidence for dual-active intermediates in iron-catalyzed water oxidation. *Angew. Chem., Int. Ed.* **2013**, *52*, 1789−1791.
(45) Lin, Y.; Zhou, S.; Sheehan, S. W.; Wang, D. Nanonet-based hematite heteronanostructures for efficient solar water splitting. *J. Am. Chem. Soc.* **2011**, *133*, 2398−2401.
(46) Mayer, M. T.; Du, C.; Wang, D. Hematite/Si nanowire dual-absorber system for photoelectrochemical water splitting at low applied potentials. *J. Am. Chem. Soc.* **2012**, *134*, 12406−12409.
(47) Young, K. M. H.; Klahr, B. M.; Zandi, O.; Hamann, T. W. Photocatalytic water oxidation with hematite electrodes. *Catal. Sci. Technol.* **2013**, *3*, 1660.
(48) Fukuzumi, S.; Hong, D. Homogeneous versus Heterogeneous Catalysts in Water Oxidation. *Eur. J. Inorg. Chem.* **2014**, 645−659.
(49) Schley, N. D.; Blakemore, J. D.; Subbaiyan, N. K.; Incarvito, C. D.; D'Souza, F.; Crabtree, R. H.; Brudvig, G. W. Distinguishing Homogeneous from Heterogeneous Catalysis in Electrode-Driven Water Oxidation with Molecular Iridium Complexes. *J. Am. Chem. Soc.* **2011**, *133*, 10473−10481.
(50) van der Ham, C. J. M.; Işık, F.; Verhoeven, T. W. G. M.; Niemantsverdriet, J. W.; Hetterscheid, D. G. H. Activation pathways taking place at molecular copper precatalysts for the oxygen evolution reaction. *Catal. Today* **2017**, *290*, 33−38.
(51) Hetterscheid, D. G. H. In operando studies on the electrochemical oxidation of water mediated by molecular catalysts. *Chem. Commun.* **2017**, *53*, 10622−10631.
(52) Schley, N. D.; Blakemore, J. D.; Subbaiyan, N. K.; Incarvito, C. D.; D'Souza, F.; Crabtree, R. H.; Brudvig, G. W. Distinguishing homogeneous from heterogeneous catalysis in electrode-driven water oxidation with molecular iridium complexes. *J. Am. Chem. Soc.* **2011**, *133*, 10473−10481.
(53) Wonders, A. H.; Housmans, T. H. M.; Rosca, V.; Koper, M. T. M. On-line mass spectrometry system for measurements at single-crystal electrodes in hanging meniscus configuration. *J. Appl. Electrochem.* **2006**, *36*, 1215−1221.
(54) Abril, P.; del Río, M. P.; Tejel, C.; Verhoeven, T. W. G. M.; Niemantsverdriet, J. W. H.; Van der Ham, C. J. M.; Kottrup, K. G.; Hetterscheid, D. G. H. Detangling Catalyst Modification Reactions from the Oxygen Evolution Reaction by Online Mass Spectrometry. *ACS Catal.* **2016**, *6*, 7872−7875.
(55) Hintermair, U.; Sheehan, S. W.; Parent, A. R.; Ess, D. H.; Richens, D. T.; Vaccaro, P. H.; Brudvig, G. W.; Crabtree, R. H. Precursor transformation during molecular oxidation catalysis with organometallic iridium complexes. *J. Am. Chem. Soc.* **2013**, *135*, 10837−10851.
(56) Limburg, B.; Bouwman, E.; Bonnet, S. Molecular water oxidation catalysts based on transition metals and their decomposition pathways. *Coord. Chem. Rev.* **2012**, *256*, 1451−1467.

https://dx.doi.org/10.1021/acscatal.0c05439
ACS Catal. 2021, 11, 2583−2595

(57) Esarey, S. L.; Holland, J. C.; Bartlett, B. M. Determining the Fate of a Non-Heme Iron Oxidation Catalyst Under Illumination, Oxygen, and Acid. *Inorg. Chem.* **2016**, *55*, 11040−11049.
(58) Lee, W.-T.; Muñoz, S. B., III; Dickie, D. A.; Smith, J. M. Ligand Modification Transforms a Catalase Mimic into a Water Oxidation Catalyst. *Angew. Chem., Int. Ed.* **2014**, *53*, 9856−9859.
(59) Costas, M.; Que, L., Jr. Lawrence Ligand Topology Tuning of Iron-Catalyzed Hydrocarbon Oxidations. *Angew. Chem., Int. Ed.* **2002**, *41*, 2179−2181.
(60) Murphy, A.; Dubois, G.; Stack, T. D. P. Efficient Epoxidation of Electron-Deficient Olefins with a Cationic Manganese Complex. *J. Am. Chem. Soc.* **2003**, *125*, 5250−5251.
(61) Chen, M. S.; White, M. C. A Predictably Selective Aliphatic C−H Oxidation Reaction for Complex Molecule Synthesis. *Science* **2007**, *318*, 783−787.
(62) Garcia-Bosch, I.; Ribas, X.; Costas, M. A Broad Substrate-Scope Method for Fast, Efficient and Selective Hydrogen Peroxide-Epoxidation. *Adv. Synth. Catal.* **2009**, *351*, 348−352.
(63) Ottenbacher, R. V.; Samsonenko, D. G.; Talsi, E. P.; Bryliakov, K. P. Highly Efficient, Regioselective, and Stereospecific Oxidation of Aliphatic C−H Groups with H_2O_2, Catalyzed by Aminopyridine Manganese Complexes. *Org. Lett.* **2012**, *14*, 4310−4313.
(64) Ottenbacher, R. V.; Talsi, E. P.; Bryliakov, K. P. Mechanism of Selective C−H Hydroxylation Mediated by Manganese Amino-pyridine Enzyme Models. *ACS Catal.* **2015**, *5*, 39−44.
(65) Dantignana, V.; Milan, M.; Cussó, O.; Company, A.; Bietti, M.; Costas, M. Chemoselective Aliphatic C−H Bond Oxidation Enabled by Polarity Reversal. *ACS Cent. Sci.* **2017**, *3*, 1350−1358.
(66) Milan, M.; Bietti, M.; Costas, M. Highly Enantioselective Oxidation of Nonactivated Aliphatic C−H Bonds with Hydrogen Peroxide Catalyzed by Manganese Complexes. *ACS Cent. Sci.* **2017**, *3*, 196−204.
(67) Najafpour, M. M.; Renger, G.; Hołyńska, M.; Moghaddam, A. N.; Aro, E.-M.; Carpentier, R.; Nishihara, H.; Eaton-Rye, J. J.; Shen, J.-R.; Allakhverdiev, S. I. Manganese Compounds as Water-Oxidizing Catalysts: From the Natural Water-Oxidizing Complex to Nanosized Manganese Oxide Structures. *Chem. Rev.* **2016**, *116*, 2886−2936.
(68) Shimazaki, Y.; Nagano, T.; Takesue, H.; Ye, B.-H.; Tani, F.; Naruta, Y. Characterization of a Dinuclear Mn^{V}=O Complex and Its Efficient Evolution of O_2 in the Presence of Water. *Angew. Chem., Int. Ed.* **2004**, *43*, 98−100.
(69) Hocking, R. K.; Brimblecombe, R.; Chang, L.-Y.; Singh, A.; Cheah, M. H.; Glover, C.; Casey, W. H.; Spiccia, L. Water-oxidation catalysis by manganese in a geochemical-like cycle. *Nat. Chem.* **2011**, *3*, 461−466.
(70) Zaharieva, I.; Chernev, P.; Risch, M.; Klingan, K.; Kohlhoff, M.; Fischer, A.; Dau, H. Electrosynthesis, functional, and structural characterization of a water-oxidizing manganese oxide. *Energy Environ. Sci.* **2012**, *5*, 7081−7089.
(71) Gorlin, Y.; Lassalle-Kaiser, B.; Benck, J. D.; Gul, S.; Webb, S. M.; Yachandra, V. K.; Yano, J.; Jaramillo, T. F. In Situ X-ray Absorption Spectroscopy Investigation of a Bifunctional Manganese Oxide Catalyst with High Activity for Electrochemical Water Oxidation and Oxygen Reduction. *J. Am. Chem. Soc.* **2013**, *135*, 8525−8534.
(72) Wang, D.; Ray, K.; Collins, M. J.; Farquhar, E. R.; Frisch, J. R.; Gómez, L.; Jackson, T. A.; Kerscher, M.; Waleska, A.; Comba, P.; Costas, M.; Que, L. Nonheme oxoiron(IV) complexes of pentadentate N5 ligands: spectroscopy, electrochemistry, and oxidative reactivity. *Chem. Sci.* **2013**, *4*, 282−291.
(73) Acuña-Parés, F.; Codolà, Z.; Costas, M.; Luis, J. M.; Lloret-Fillol, J. Unraveling the Mechanism of Water Oxidation Catalyzed by Nonheme Iron Complexes. *Chem.—Eur. J.* **2014**, *20*, 5696−5707.
(74) Acuña-Parés, F.; Costas, M.; Luis, J. M.; Lloret-Fillol, J. Theoretical Study of the Water Oxidation Mechanism with Non-heme Fe(Pytacn) Iron Complexes. Evidence That the Fe^{IV}(O)-(Pytacn) Species Cannot React with the Water Molecule To Form the O−O Bond. *Inorg. Chem.* **2014**, *53*, 5474−5485.
(75) Koepke, S. J.; Light, K. M.; VanNatta, P. E.; Wiley, K. M.; Kieber-Emmons, M. T. Electrocatalytic Water Oxidation by a Homogeneous Copper Catalyst Disfavors Single-Site Mechanisms. *J. Am. Chem. Soc.* **2017**, *139*, 8586−8600.

https://dx.doi.org/10.1021/acscatal.0c05439
ACS Catal. 2021, 11, 2583−2595